Parking Lot Measurement with 24 GHz Short Range Automotive Radar

Andreas Loeffler*, **Julian Ronczka****, **Thomas Fechner***

*Division Chassis & Safety, BU ADAS, Continental
Peter-Dornier-Str., 10, 88131 Lindau, GERMANY
email: {andreas.3.loeffler, thomas.fechner}@continental-corporation.com

**Automotive - Cross Divisional Functions, Continental Engineering Services, Continental
Graf - Vollrath - Weg, 6, 60489 Frankfurt/Main, GERMANY
email: julian.ronczka@conti-engineering.com

Abstract: *This paper focuses on automotive 24 GHz radar sensors used for measuring parking lots. The parking lot detection is based upon an occupancy grid featuring Dempster-Shafer theory. The grid is filled with information of static clusters measured by the sensors. Two compensating factors are introduced to improve the reconstruction of the surroundings of the vehicle. Measurement results presented at the end of the paper show that even at higher vehicle speeds it is possible to detect parking lots on the other side of the road.*

1. Introduction

The search for free parking spaces without affecting seriously the traffic flow is a major issue as parking spaces in cities are becoming fewer and fewer. Particularly in small roads with parallel parking spaces in combination with a high traffic volume, it is mandatory to find an appropriate parking lot at higher speeds (up to 60 km/h) and perform the corresponding parking, accordingly. Modern cars are equipped with different kinds of sensors, e.g. optical, ultrasonic and radar sensors. Finding parking spaces with optical sensors (camera sensor) requires at minimum a lateral view [1] or even a surround view, e.g. provided by several fish-eye cameras [2]. Although these sensors could obtain high resolution, still, they are subject to environmental pollution and light conditions. Ultrasonic sensors are widely used for parking applications because of small costs [3, 4]. However, ultrasonic sensors have several disadvantages regarding the above mentioned scenario, apart from also being subject to environmental influences. The range of ultrasonic sensors is limited, also depending on the speed of the vehicle. Tests showed that ultrasonic based park assists are partly not able to detect obstacles like barrier chains, high curbstones and protective hoops (e.g., for tree protection). The above mentioned issues could be bypassed by using a short range radar sensor (SRR sensor) instead or in addition to existing parking aid sensors.

In our work we evaluate an SRR sensor working at 24 GHz, providing a range gate length of around 40 cm. Static cluster measurements of the sensor are evaluated to provide an occupancy

grid [5, 6] based on the Dempster-Shafer theory (DST) [7]. The current grid cell size is fixed to 10 cm × 10 cm and every static cluster is formed on the grid using a 2D Gaussian distribution defining the probability for *occupied*, *free* and *unknown*.

The remainder of the paper is organized as follows. The following Section gives some insights into the SRR sensor used and how the occupancy grid is filled. Section 3 describes the parking scenarios and Section 4 shows the results obtained from the application of the occupancy grid to real sensor measurements.

2. Sensor and Occupancy Grid

The radar sensors used for this approach are referred to as short range radar sensors working at 24 GHz and occupying a net bandwidth of around 375 MHz (extended 24 GHz band usage with guard interval) leading to a range gate length of 40 cm and an accuracy of 8 cm. This kind of sensor is widely deployed, e.g. in existing blind spot detection (BSD), lane change assist (LCA) and cross traffic alert (CTA) applications. Four sensors, attached at each corner of the vehicle (front left and right, rear left and right), create an overall field of view (FOV) around the vehicle. Each sensor has a single FOV of around 150° and is tilted horizontally ±63° (left and right front sensor) respectively ±115 ° (left and right rear sensor) w.r.t. the forward-facing vehicle. The sensor's measurement interface provide a special set of measurement data from which we are using the provided static cluster list. This list includes (among other quantities) at the sensor's interval of 40 ms:

- the current timestamp of the sensor
- the number of static clusters (consolidated scattering points),
- the measured range (in m) and angle (in rad) of a specific cluster within the cluster list and
- the measured radar cross section (RCS in $dBsm$) of each cluster.

These quantities are used to provide data for filling the occupancy grid [8]. The occupancy grid used is based on a grid cell size of currently 10 cm × 10 cm. According to particular applications the grid cell size may be increased (for better computing) or decreased (for higher resolution). The quadratic map itself has an edge length of 90 m. The theoretical probability approach of the grid is based on the Dempster-Shafer theory, i.e. extending the Bayesian approach ($free$ and $occupied$ cells) [9] by introducing a frame of discernment (FOD) Θ which involves a finite set of mutually exclusive and completive probabilistic statements. According to that theory the value for the FOD for a given cell C at coordinates xy with probabilities for free $free$ and occupied occ is defined as $\Theta = (free, occ)$. Accordingly, the complete set of probabilistic statements 2^{Θ} includes

$$2^{\Theta} = \{\emptyset, free, occ, (free, occ)\} \tag{1}$$

whereas $free$, occ and $(free, occ) = \Theta$ define the statements that the cell C_{xy} is *free*, *occupied* and in *unknown* state. The null proposition $\emptyset$ is set to zero as it corresponds to *no statement*. The mass m_{xy} in this theory is referred to as the degree of belief [10] with the sum of all masses for each cell C_{xy} being one:

$$\sum_{P \in 2^{\Theta}} m_{xy}\left\{P\right\} = m_{xy,M}\left\{\emptyset\right\} + m_{xy,M}\left\{free\right\} + m_{xy,M}\left\{occ\right\} + m_{xy,M}\left\{\Theta\right\} = 1 \tag{2}$$

The mass of a certain cell m_{xy} defines the probability of the proposition (free, occupied, unknown). Subsequently, the map M with its cells C_{xy} is initialized with

$$m_{xy,M}\left\{\emptyset\right\} = 0,\ m_{xy,M}\left\{free\right\} = 0,\ m_{xy,M}\left\{occ\right\} = 0,\ m_{xy,M}\left\{(free, occ)\right\} = 1, \forall C_{xy} \in M \tag{3}$$

Updating the map M with sensor measurements is done according to Dempster's rule of combination. Each sensor measurement generates a new sensor map S with appropriate occupancy probabilities (see details below). The coordinates of the sensor map are transformed to global map coordinates and both maps, i.e., M and S are updated according to (4), creating the updated map M'.

$$\begin{aligned} m_{xy,M'}\left\{free\right\} = \\ \frac{m_{xy,M}\left\{free\right\} \cdot m_{xy,S}\left\{free\right\} + m_{xy,M}\left\{free\right\} \cdot m_{xy,S}\left\{\Theta\right\} + m_{xy,S}\left\{free\right\} \cdot m_{xy,M}\left\{\Theta\right\}}{1 - \left(m_{xy,M}\left\{free\right\} \cdot m_{xy,S}\left\{occ\right\} + m_{xy,M}\left\{occ\right\} \cdot m_{xy,S}\left\{free\right\}\right)} \\ m_{xy,M'}\left\{occ\right\} = \\ \frac{m_{xy,M}\left\{occ\right\} \cdot m_{xy,S}\left\{occ\right\} + m_{xy,M}\left\{occ\right\} \cdot m_{xy,S}\left\{\Theta\right\} + m_{xy,S}\left\{occ\right\} \cdot m_{xy,M}\left\{\Theta\right\}}{1 - \left(m_{xy,M}\left\{free\right\} \cdot m_{xy,S}\left\{occ\right\} + m_{xy,M}\left\{occ\right\} \cdot m_{xy,S}\left\{free\right\}\right)} \end{aligned} \tag{4}$$

The next step is to transform the static clusters into the DST grid. In the current approach this is realized by modeling each cluster as Gaussian distribution for the hypothesis *occupied* in radial (w.r.t. range) and azimuthal (w.r.t. angle) direction [5] specifying the occupancy mass $m_{xy}\left\{occ\right\}$. Let us assume a measured cluster with azimuth angle φ and range r. The standard deviations for azimuthal and radial directions are defined as σ_{φ} and σ_r. The distance and angle between the sensor and the map cells C_{xy} are given as r_{xy} and φ_{xy}, the map cell size in azimuthal and radial direction is determined as d_{φ} and d_r. The cumulative distribution function (cdf) of the Gaussian distribution $\mathcal{N}(\mu, \sigma)$ is defined as

$$\Phi_{\mathcal{N}(\mu,\sigma)}(x) = \frac{1}{2}\left(1 + \operatorname{erf}\left(\frac{x-\mu}{\sqrt{2}\sigma}\right)\right) \text{ with } \operatorname{erf}(a) = \frac{2}{\sqrt{\pi}} \int_0^a e^{-t^2} \mathrm{d}t \tag{5}$$

In order to calculate the occupancy masses $m_{xy}\left\{occ\right\}$ for each cell, we first calculate the Gaussian factors $f_{\varphi,xy}$ and $f_{r,xy}$ for azimuth and range over each cell with

$$f_{\varphi,xy} = \Phi_{\mathcal{N}(\mu=\varphi_{xy},\sigma_{\varphi})}\left(\varphi + \frac{1}{2}d_{\varphi}\right) - \Phi_{\mathcal{N}(\mu=\varphi_{xy},\sigma_{\varphi})}\left(\varphi - \frac{1}{2}d_{\varphi}\right) \tag{6}$$

$$f_{r,xy} = \Phi_{\mathcal{N}(\mu=r_{xy},\sigma_r)}\left(r + d_r\right) - \Phi_{\mathcal{N}(\mu=r_{xy},\sigma_r)}\left(r\right) \tag{7}$$

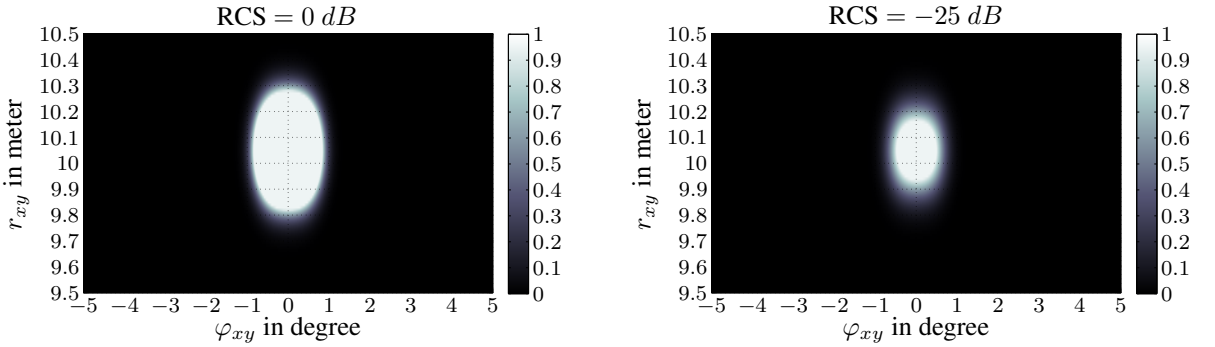

Figure 1: Results of simulated Gaussian curves for a cluster at $\varphi = 0°$ and $r = 10\ m$, considering the RCS factor $\Delta\sigma_{\text{RCS}}$ for clusters with RCS values of $0\ dB$ and $-25\ dB$

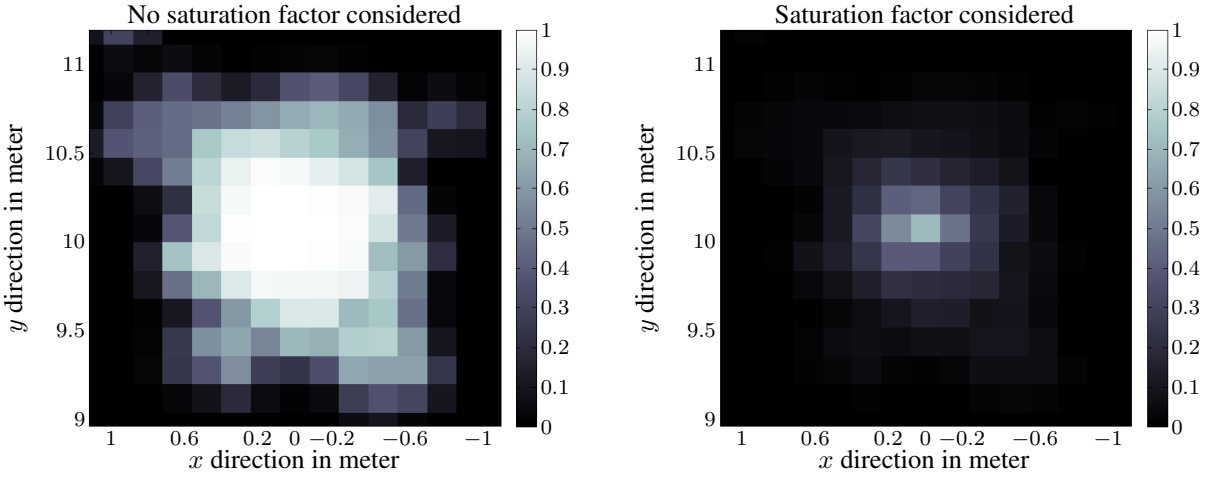

Figure 2: Grid results of simulated Gaussian curves for a cluster at $x = 0\ m$ and $y = 10\ m$, with and without consideration of the saturation factor m_{sat} over several simulated sensor measurements

The occupancy for a specific grid $m_{xy}\{occ\}$ is now calculated by combining the Gaussian factors

$$m_{xy}\{occ\} = f_{\varphi,xy} \cdot f_{r,xy} \cdot \Delta\sigma_{\text{RCS}} \cdot m_{\text{sat}}, \tag{8}$$

the occupancy for free is defined as zero, i.e. $m_{xy}\{free\} = 0$. The factors $\Delta\sigma_{\text{RCS}}$ and m_{sat} in (8) are referred to as RCS factor and saturation factor. The latter factor m_{sat} is introduced to confirm an existing *occupied state* with higher probability than a *free* or *unknown state*, i.e. a occupied cell will be more likely confirmed as further occupied than a non-occupied cell. The former factor is used to weight the occupancy with the RCS value of the cluster meaning the higher the RCS value, the higher the occupancy probability is. Figures 1 and 2 show simulated results of the occupancy grid. However, it is only shown the probability for *occupied* in the range of $[0; 1]$. Fig. 1 shows results for the occupancy of a cluster ($\varphi = 0°$ and $r = 10\ m$) for different RCS values ($0\ dB$ and $-25\ dB$). The standard deviations are given with $\sigma_\varphi = 1°$ and $\sigma_r = 0.1\ m$, the polar grid cell sizes are defined as $d_\varphi = 1°$ and $d_r = 0.1\ m$. Fig. 2 shows the simulated results of the occupancy grid considering the saturation factor m_{sat}. In that case the simulated sensor measurement of φ and r is disturbed by adding Gaussian distributed noise

with arbitrary chosen standard deviations of $\sigma_{\varphi,\text{meas}} = 2°$ and $\sigma_{r,\text{meas}} = 0.2\ m$. The saturation factor makes sure that already as occupied declared grid cells keep their occupied state, whereas only once as occupied considered cells are rather suppressed. The effect can be directly seen from the figure. Because of the noisy measurements, basically, the occupancy probability is distributed around the expectation value. If the saturation factor is not taken into account, the grid is filled accordingly (Fig. 2, left) resulting in a widespread occupancy. By considering the saturation factor (Fig. 2, right) it can be noticed that the spreading effect is strongly suppressed depending on the chosen saturation curve. Therefore, the introduction of the saturation factor takes the effect of noisy measurements into account.

3. Results from Real Measurements

This section includes obtained results from real world measurements. The vehicle used is equipped with four SRR sensors. The shown scenario (Fig. 3a) was recorded at a velocity of $v_{\text{car}} = 40\ km/h$. The vehicle pose updates are performed timestamp-wise using speed and accumulated yaw rate. The results of the measurements (see Fig. 3b, 3c, 3d) show a very accurate reproduction of the reality when compared to the given scenario. The red color represents the probability of *occupied*, the green color of *free* and black refers to *unknown*. The parking vehicles are captured with an error around 40 cm (without RCS and saturation factor) and 20 cm (with RCS and saturation factor) resulting in detected vehicles larger than in reality. This error

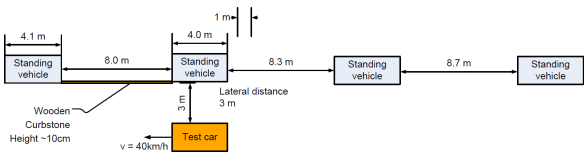

(a) Parking scene

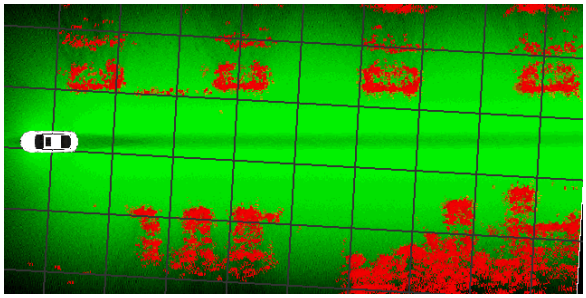

(b) Results: w/o RCS and w/o saturation factor

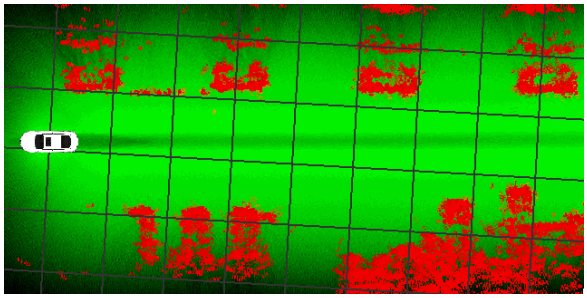

(c) Results: w/ RCS and w/o saturation factor

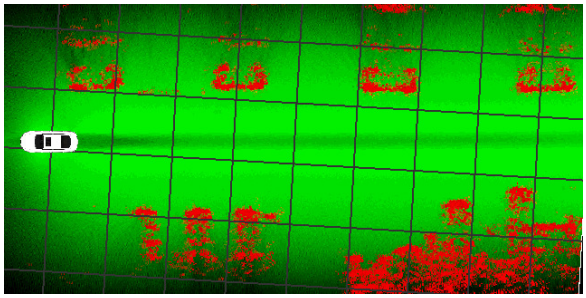

(d) Results: w/ RCS and w/ saturation factor

Figure 3: Measurement results of 4 SRR sensors for a parallel parking scenario with various usages of RCS and saturation factor (RCS threshold $= -30\ dBsm$). 3a: Parking scenario. 3b: Result without RCS and without saturation factor. 3c: Only RCS factor. 3d: RCS and saturation factor considered. The shown rough grid is $5\ m \times 5\ m$

will limit the available parking lots, however, it is preferable to ignore one free parking lot rather than to drive into an occupied one. Additionally, the parking lot detection at a lateral distance of $3\ m$ between the driving and the standing vehicles shows, that even parking lots on the other side of the road may be detected.

4. Conclusion

This paper introduced a grid-based approach to detect parking lots including four 24 GHz short range radar sensors. The static cluster information of the sensors is used to fill an occupancy grid. Two compensating factors have been introduced to enhance the final reconstruction of the free and occupied parking lots in the surroundings of the vehicle. Conducted measurements showed that even at higher vehicle speeds (e.g., 40 km/h) parking lots may be detected at the other side of the road.

References

[1] C. Unger, E. Wahl, and S. Ilic, "Parking assistance using dense motion-stereo," *Machine Vision and Applications*, vol. 25, no. 3, pp. 561–581, 2014.

[2] S. Li and Y. Hai, "Easy Calibration of a Blind-Spot-Free Fisheye Camera System Using a Scene of a Parking Space," *Intelligent Transportation Systems, IEEE Transactions on*, vol. 12, no. 1, pp. 232–242, March 2011.

[3] J. Mure-Dubois, F. Vincent, and D. Bonacci, "Sonar and radar SAR processing for parking lot detection," in *Radar Symposium (IRS), 2011 Proceedings International*, Sept 2011, pp. 471–476.

[4] W.-J. Park, B.-S. Kim, D.-E. Seo, D.-S. Kim, and K.-H. Lee, "Parking space detection using ultrasonic sensor in parking assistance system," in *Intelligent Vehicles Symposium, 2008 IEEE*, June 2008, pp. 1039–1044.

[5] A. Elfes, "Using Occupancy Grids for Mobile Robot Perception and Navigation," *Computer*, vol. 22, no. 6, pp. 46–57, June 1989.

[6] A. Schultz and W. Adams, "Continuous localization using evidence grids," in *Robotics and Automation, 1998. Proceedings. 1998 IEEE International Conference on*, vol. 4, May 1998, pp. 2833–2839 vol.4.

[7] G. Shafer, *A mathematical theory of evidence*. Princeton University Press, 1976, vol. 1.

[8] R. Grewe, A. Hohm, S. Hegemann, S. Lueke, and H. Winner, "Towards a generic and efficient environment model for ADAS," in *Intelligent Vehicles Symposium (IV), 2012 IEEE*, June 2012, pp. 316–321.

[9] A. Elfes, "Occupancy Grids: A Stochastic Spatial Representation for Active Robot Perception," *CoRR*, vol. abs/1304.1098, 2013.

[10] D. Pagac, E. Nebot, and H. Durrant-Whyte, "An evidential approach to map-building for autonomous vehicles," *Robotics and Automation, IEEE Transactions on*, vol. 14, no. 4, pp. 623–629, Aug 1998.